Geophysical Journal International

Geophys. J. Int. (2011) **187,** 848–860 doi: 10.1111/j.1365-246X.2011.05171.x

In situ monitoring of rock fracturing using shear wave splitting analysis: an example from a mining setting

Andreas Wuestefeld,[1]* J. Michael Kendall[1] James P. Verdon,[1] and Andre van As[2]

[1]*Department of Earth Sciences, University of Bristol, Queens Road,* BS8 1RJ, *Bristol, UK. E-mail: andreas.wuestefeld@web.de*
[2]*Rio Tinto Technology & Innovation, Brisbane, Australia*

Accepted 2011 July 27. Received 2011 July 23; in original form 2011 January 12

SUMMARY

Changing stress conditions are well known to cause rupturing of rock. This is well constrained on a small scale from laboratory experiments and inferred on a much larger scale from tectonic earthquakes. Here, we present a study of rock fracturing induced by changes in stress state during block-caving operations in an Australian mine. This intermediate-scale study provides further evidence of the scalability of processes involved in rock fracturing and thus helps to link laboratory and seismological observations. We analyse the temporal evolution of rock fracturing during a production cycle using the analysis of fracture-induced anisotropy.

Fracturing of the rock mass is monitored using evidence of seismic anisotropy from estimates of shear wave splitting and their subsequent inversion for fracture parameters. The data set consists of more than 40 000 three-component seismograms recorded by an array of sensors, which provides excellent ray coverage. We applied a novel automatic quality assessment technique to handle this large data set and find that anisotropy, and thus fracturing, correlates strongly with the excavation process. We then perform a grid search over a series of synthetic models based on rock physics to invert the splitting parameters for fracture orientation and density. Finally, by applying a sliding window on our results, we are able to identify production related fracture evolution. During production the fracture density increases, with horizontal fracture density being stronger than the vertical fracture density. This can be explained by the removal of the supporting rock during caving. During short intervals of reduced production, the horizontal fracture density decreases, whereas vertical fracture density increases. We relate this to change in stress regime with reducing overburden mass during cavity collapse. This scenario is similar to a collapsing caldera or the inverse of an inflating magma chamber.

Key words: Downhole methods; Fracture and flow; Seismic anisotrophy.

1 INTRODUCTION

Fracturing of rock occurs on scales ranging from the microscale (microcracks) to the continental scale (megafaults). However, several observations indicate that these various scales of fractures are related: in laboratory experiments, it is observed that fracturing on micrometre scale is preceded by swarms of microfissures accumulating into microcracks and thus forming a fracture (e.g. Brace *et al.* 1966; Gay & Ortlepp 1979; Reches & Lockner 1994; Haimson 2007). This is also observed on the millimetre scale of rock specimen in the distribution of event locations (e.g. Lockner 1994). On a (multi) kilometre scale, seismology offers the well-established Gutenberg–Richter (1944) relationship, which states that the frequency of occurrence and the magnitude of seismic events follows a power law. Recently, this relationship has been confirmed down to rupture lengths on the centimetre scale (Boettcher *et al.* 2009; Kwiatek *et al.* 2010). Although the underlying reasons are still being debated (e.g. Wesnousky 1994; Parsons & Geist 2009), this implies that exponentially more small fractures exist than larger. Cumulating such observations suggest that macroscopic fracturing is a consequence of accumulations of ruptures at lesser scales (Allegre *et al*. 1982).

Recent increases of exploration investment in the oil and mining industry have opened the possibility of filling the gap between laboratory scale (micrometres and millimetres) and tectonic features (kilometres) by generating high quality, multicomponent seismic data sets of regions on a detailed scale. The seismic methods developed for global seismology can be easily transferred to microseismic studies. These techniques include the location of events, and determination of magnitude and faulting mechanisms. Passive seismic monitoring of anthropogenic (i.e. production related) microseismicity is gaining interest in the hydrocarbon industry (e.g. Phillips *et al.*

*Now at: ESG Solutions, 20 Hyperion Court, Kingston, K7K 7K2, Canada.

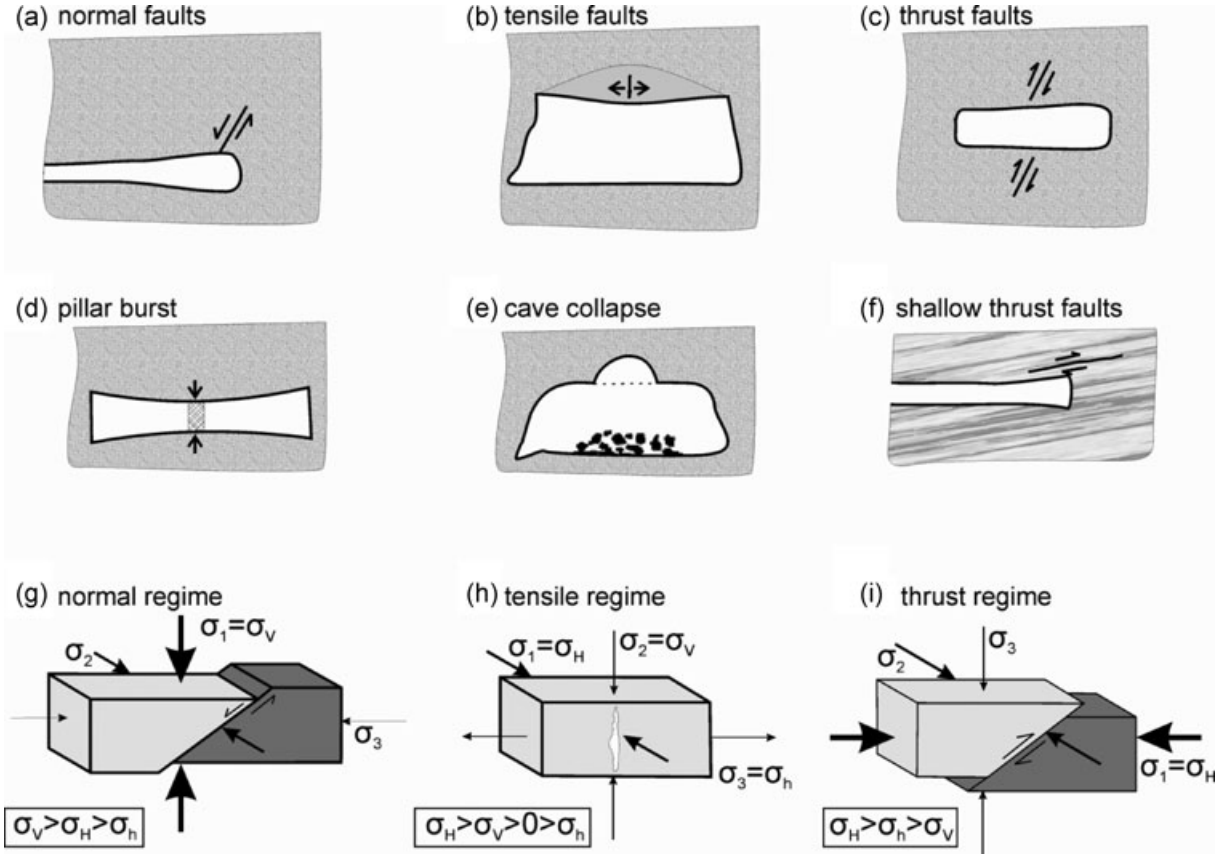

Figure 1. (a)–(f) fracture mechanisms encountered in mining environment (Hasegawa *et al.* 1989). (g)–(i) stress regimes associated with faulting.

1998, 2002; Teanby *et al.* 2004a), CO_2 storage (e.g. Verdon *et al.* 2010), geothermal projects (e.g. Rial *et al.* 2005; Baisch *et al.* 2009; Dorbath *et al.* 2009;) and mining projects (e.g. Holmes *et al.* 1993, 2000; Gibowicz & Kijko 1994; Julia *et al.* 2009; Kuehn *et al.* 2009; Plenkers *et al.* 2010). Simultaneously, the legal aspects of such induced seismicity are being discussed in the scientific community (Cypser & Davis 1998).

Microseismic studies in hydrocarbon reservoirs are intended to increase the understanding of local state of stress and the orientation and evolution of the fracture network. The knowledge of dominant crack orientation and crack density may ultimately increase productivity of an oil reservoir by optimizing the locations of injection and production wells. In a block cave mine, crack and fracture orientation is a major factor in the caveability and fragmentation of the rock mass. Furthermore, in stopping operations, productivity can be increased if production follows naturally preferred orientations. The underlying assumptions and models of stress conditions used in mining are identical to those in volcanology when studying caldera collapse or inverse to the problem of an inflating magma chamber as an eruption precursor (e.g. Gudmundson 2006).

Six potential models are conceivable for induced seismicity in mines and cavities (Fig. 1). Hasegawa *et al.* (1989) describe their mechanisms as follows (see also Brady & Brown 1985; Jaeger *et al.* 2007):

(1) A cavity collapse occurs either as a downward-oriented rockburst or as disintegration of previously loosened rock due to gravity.

(2) A pillar burst represents the shear failure of a pillar due to changing stress conditions following the advancement of the stope face.

(3) Tensile failure above the cave may occur near the middle of a wide excavation. This may be due to elastic bending of the cap rock due to the gravitational force of the overburden.

(4) The most common type of fracturing is (steeply dipping) normal faulting due to stress concentrations at the stope front.

(5) Thrusting above or below a cave if the maximum principal stress is horizontal and the (induced) decrease in vertical stress is large enough to initiate (shallow dipping) rock failure.

(6) Finally shallow, near-horizontal thrusting above a cave can occur where near-horizontal layers of rocks loosen or experience shearing due to the flexure of the cave roof.

Monitoring of seismicity in mines probably started with the installation of a seismograph in the Ruhr coal basin in Germany (Mintrop 1909). Since then, the understanding of induced seismicity has improved greatly (e.g. Simpson 1986; Gibowicz & Kijko 1994; Phillips *et al.* 2002). Engineering activities cause the redistribution of crustal stresses. At locations where the shear stress exceeds the Mohr–Coulomb failure criterion (Jaeger *et al.* 2007) this stress redistribution results in failure of the rock, which can be recorded as microsesmicity. Long-term monitoring of microseismicity has the potential to reveal fracture geometry (e.g. Phillips *et al.* 1998, 2002; Spottiswood & Milev 1998; Urbancic & Rutledge 2000). The determination of detailed hypocentre moment tensor solution for microearthquakes may provide more detailed understanding of fracturing processes (e.g. Hasegawa *et al.* 1989; Trifu *et al.* 2000; Boettcher *et al.* 2009; Julia *et al.* 2009; Kuehn *et al.* 2009). It is noteworthy that the mining industry often distinguishes two types of rock failure situations (e.g. McGarr 1971a,b): rockbursts directly damage excavations, whereas seismic events are regarded as

non-destructive to the excavation wall, but fracture the rock internally and thus influencing rock stability. Especially, rockbursts pose a major risk to mine personnel and may also adversely affect the productivity of a mine. For mining operations, being able to monitor the seismic activity helps to track the propagation of the cave as well as identify potential hazards in operational areas and act accordingly (Potvin 2009). To date, evaluation of rock stability often depends on the experience of operators and engineers (Mikula 2005), and the use of advanced seismic techniques such as moment tensors or shear wave splitting as tools for objective decision making are only recently attracting the operators.

An emerging new approach to fracture characterization is the analysis of shear wave anisotropy. Shear wave splitting occurs if a seismic shear wave enters an anisotropic medium (e.g. Nur & Simmons 1969; Crampin 1984; Savage 1999). The shear wave is split into two orthogonally polarized shear waves, whose orientations are associated with the symmetry of anisotropy. The two waves are separated by a delay time, proportional to the strength of anisotropy and the length of the travel path within the anisotropic medium. The anisotropy can be due to aligned fractures (e.g. Crampin 1984; Kendall *et al.* 2006; Schoenberg 2009), periodic layering (Backus 1965), alignment of anisotropic minerals (e.g. Blackman *et al.* 2002; Valcke *et al.* 2006) or local-stress aligned microcracks (Vega *et al.* 2006; Hall *et al.* 2008; Verdon *et al.* 2008). Shear wave splitting has been successfully applied to mantle tectonics on global (e.g. Silver 1996; Barruol & Hofmann 1999; Savage 1999), regional (for a compilation, see Wuestefeld *et al.* 2009) or crustal scales (for a review, see Crampin & Peacock 2008). These studies mainly aim to understand tectonic processes.

With industrial applications, shear wave splitting can add valuable insight into stress-induced anisotropy and thus the geometry of cracks and fractures on a range of length scales (Teanby *et al.* 2004a; Kendall *et al.* 2006; Hall *et al.* 2008; Al-Harrasi *et al.* 2011a,b). Cracks and fractures will open and close in response to changes in the stress field; the challenge lies in understanding the contributions from different length scales. Studies of microseismicity are ideally suited to such studies, as they often offer ray coverage over a wide range of dips and azimuths. This in turn allows inversions for complex anisotropy parameters and thus complex fracture configurations (Verdon *et al.* 2009; Wuestefeld *et al.* 2010). Note that this approach assumes a homogeneous anisotropic rock mass. Observations of frequency-dependent anisotropy show promise as a means of characterizing length scales (e.g. Al-Harrasi *et al.* 2011b). Thus, monitoring temporal variations in shear wave splitting offers a useful probe of stress-related changes in the evolution of crack and fracture networks.

Here, we present shear wave splitting analysis of microseismic data recorded at E26 Lift 2 block cave of the porphyry copper–gold Northparkes Mines (Australia), operated by Rio Tinto. Block caving is a mining method that exploits the gravitational potential of a naturally fractured rock (Brady & Brown 1985). Caving is initiated by blasting a narrow slot over a large area (the so-called undercut level) beneath the ore body to be mined. Stress redistribution and gravity cause fracturing (e.g. Simpson 1986) and caving of the ore into the undercut. As broken ore is removed, the cave enlarges progressively upwards. The main requirement is to ensure a steady displacement of caving mass so that the mined void is continuously self-filling. This can be achieved if the rock mass contains natural fractures in sufficient density such that it will naturally cave when undercut. Often, caving is assisted with targeted blasts. The caved pieces of rock cannot be too large or they will be difficult to extract from the drawpoints. Kendorski (1978) suggests that the most favourable conditions are a rock mass with two subvertical joint sets plus a subhorizontal joint set with a dip less than about 30° (see also Brady & Brown 1985). It is therefore important to understand the fracture distribution and development in the ore body.

As mentioned, systematic analysis of shear wave splitting parameters can provide detailed insight in fracture characteristics. The new, stress-induced fracture orientation is governed by the state of stress and the geometry of existing joint fabric in the rock mass and thus can be used to determine stress redistributions, which may influence cave propagation (Laubscher 1994; Trueman *et al.* 2002). If measured in real time it might even be possible to adjust the cave management strategy to try and ensure more uniform cave propagation and ultimately improve recoveries. To date, most shear wave splitting studies in reservoirs have been performed in petroleum or volcanic environments. In mining environments, shear wave splitting as a rock mass characterization tool is to the authors' knowledge limited to early studies by Holmes *et al.* (1993, 2000). This is a missed opportunity as seismic networks with good ray coverage are comparatively complex and expensive to install in hydrocarbon reservoirs, whereas galleries in mining operations allow easy access in and around the ore body, which thus provides good ray coverage required for shear wave splitting studies.

2 THE DATA SET

During the main excavation period from 2004 June to 2005 January, a total of 13 354 microseismic events with local magnitude up to +2.9 were recorded and located by an ISS International Ltd. system (Hudyma *et al.* 2007a,b). Up to 500 events per day were recorded. Fig. 2 shows the locations of seismic event and sensors.

A previous study by Hudyma *et al.* (2007b) focused on the seismic attributes (seismicity rate, event magnitudes and *b*-values), of the data set. They observe that in the early phase of excavation to 2004 mid-October the magnitudes of events are small (less then local magnitude 0) but the seismicity rate is high (Fig. 3). The authors also infer a shifting of the top of the seismogenic zone at a rate of approximately 0.5 m d^{-1}. From October 16 onwards, the top of seismogenic zone moved upward at a rate of 2.4 m d^{-1} 2 weeks, though the production rate remained constant. Following that 2-week period, the number of events decreased but event magnitude increased, with six events of local magnitude larger than +2 occurring between November 3 and 16. During this time, the top of seismogenic zone moved at a rate of almost 4 m d^{-1}. Hudyma *et al.* (2007b) attribute this to stress redistribution within the crown pillar between the monitored excavation and a previous operation above. The physical caving front lags behind the seismogenic zone. A widening of this so-called loosening zone from mid-October to mid-November indicates an increased hazard in that period. This hypothesis is supported by the fact that the seismicity reduced significantly after the breakthrough of the seismogenic front into the cave above.

Analysing *b*-values of a frequency–magnitude distribution (Gutenberg & Richter 1944) is a technique, which is widely used in seismic hazard analysis. The slope of frequency–magnitude of seismic events distribution is referred to as the *b*-value. At the Northparkes Mine, this power law is obeyed in the first part of excavation. In the period between October 17 and November 16 Hudyma *et al.* (2007b) found a bimodal frequency–magnitude relation. They relate this to different source mechanisms during breakthrough of the crown pillar. Schorlemmer *et al.* (2005) observe a change is *b*-value with focal mechanism within the regional earthquake

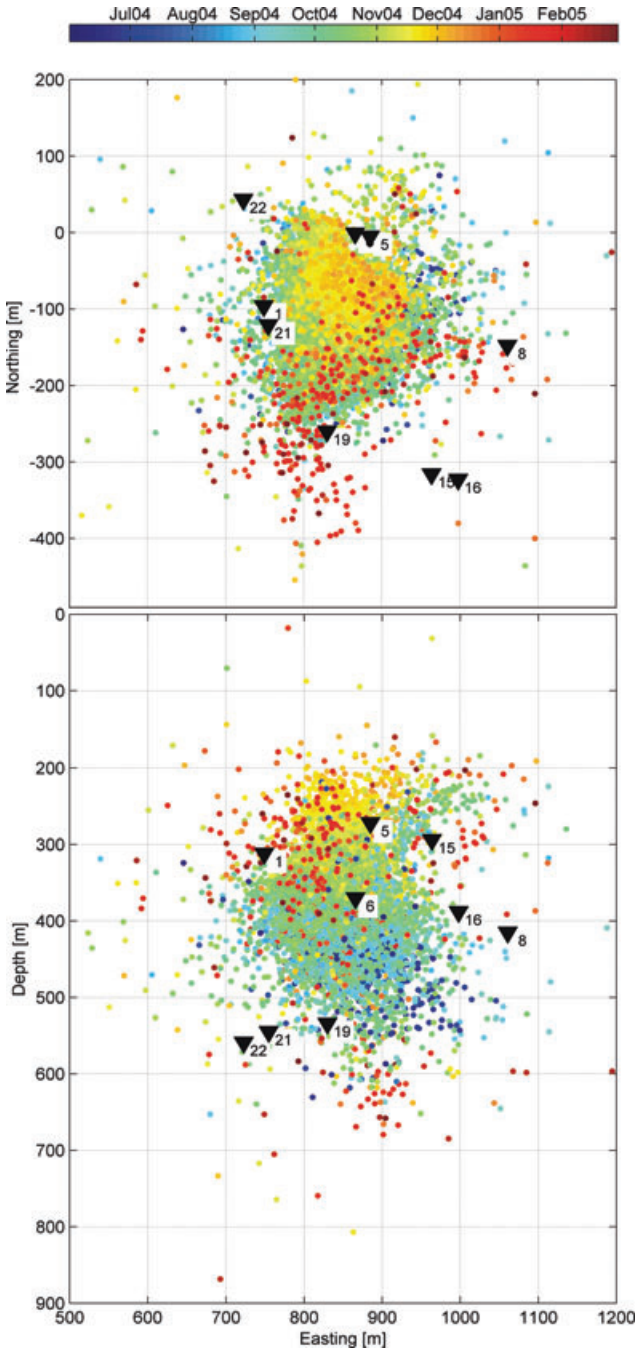

Figure 2. Location of the Northparkes events in map view (top panel) and cross-section (bottom panel). Colour indicates temporal evolution, where upward motion of events can be clearly seen in the bottom panel. Note that depth is below sea level and topographic elevation is approximately 250 m at the Northparkes Mine. Stations marked with triangles are used in this study.

catalogues, and relate that to different stress conditions required for rupture to occur, where thrust faults need higher stresses than (gravity assisted) normal. At Northparkes, a series of three-component seismometers has been placed three-dimensionally around the ore body to be caved. The ore body is assumed as a homogeneous block with seismic velocities of $v_p = 3900$ m s^{-1} and $v_s = 2575$ m s^{-1}. The directional coverage (Fig. 2) of the seismogenic zone from a large variety of azimuths and incident angles is ideal for shear wave splitting analysis. This is a great improvement to most studies up to date, where single well sensor chains have been used. Shear wave splitting requires the complete 3-D waveform (Verdon *et al.* 2009; Wuestefeld *et al.* 2010) and we thus exclude sensors with one or more dead components. The Northparkes microseismic data set thus consists of 40 586 three-components seismograms, recorded on nine sensors with manually picked *P* and *S* arrivals provided by Golder Associates, Auckland, New Zealand.

Fig. 4 shows the broad frequency range of the database. Travel path lengths vary and show a median value of 176 m. Note that the data quality in hard rock is generally higher than in typical hydrocarbon settings, where reflections and refractions from adjacent sedimentary layers often leads to complex waveforms.

The recordings showed strong periodic noise, presumably of electric origin due to faulty cable connection or the power mainframe and associated harmonics (e.g. Butler & Russelly 2003). Interestingly, the dominant noise frequency varies not only between each station or the three components, but also we observe a variation in the harmonic noise spectrum between each trace that is different for each event. We therefore applied the adaptive harmonic noise filter described in Wuestefeld *et al.* (2010), which uses the spectrum of the pre-signal noise as notch filter.

3 PROCESSING

The analysis of shear wave splitting within this large data set was performed fully automatically, using the workflow described in Wuestefeld *et al.* (2010). First, the waves are rotated into natural coordinates based on *P*-wave particle motion. Then, we perform a cluster analysis of the splitting parameters for a set of 140 possible *S*-wave windows to reduce dependency on picking accuracy and window selection (Teanby *et al.* 2004b). A quality index Q is assigned to each measurement based on characteristic differences between two independent splitting inversion techniques (Wuestefeld & Bokelmann 2007; Wuestefeld *et al.* 2010). This quality index ranges from –1 (denoting 'Null' or 'no splitting') to 0 (denoting 'Poor' measurements) to +1 (denoting 'Good' measurements). Only values above a certain threshold are used in further processing. We applied a broad-bandpass filter with corner frequencies of 150 and 1500 Hz to the signal. An example of a good splitting measurement is shown in Fig. 5. The histogram distribution of quality is shown in Fig. 6(a), whereas Fig. 6(b) shows also the quality distribution in respect of the initial polarisation of the shear wave. Note that from Fig. 6(b), it is clear that a separation between fast axis and initial polarization of approximately 20° is required for reliably obtaining a good measurement.

4 RESULTS

Processing of the Northparkes microseismic data set yielded in 40 586 shear wave splitting observations. The automation procedure described in Wuestefeld *et al.* (2010) allowed for quick and consistent processing.

Fig. 6 illustrates the quality distribution of these observations. Note the large number of high-quality ($Q > 0.8$) observations. This can be attributed to the good overall quality of the data set, which contains only those events where *P* and *S* arrivals could be handpicked and thus generally have relatively clear waveforms and an overall high signal-to-noise ratio.

When using shear wave splitting measurement, one can approximate the ray-path-dependent percentage anisotropy by

$$A = v_S * \mathrm{d}t * 100/r, \quad (1)$$

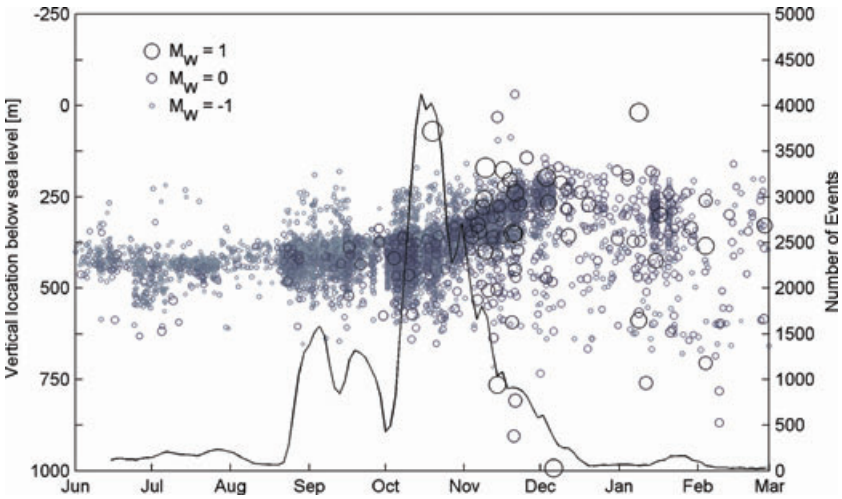

Figure 3. Magnitude and depth variation in time. Also shown, as solid line, is the number of events in a 14-d sliding window. The upward progress of the block caving can easily be seen. Note that the largest magnitude events occur during and after highest caving rate (after mid-October).

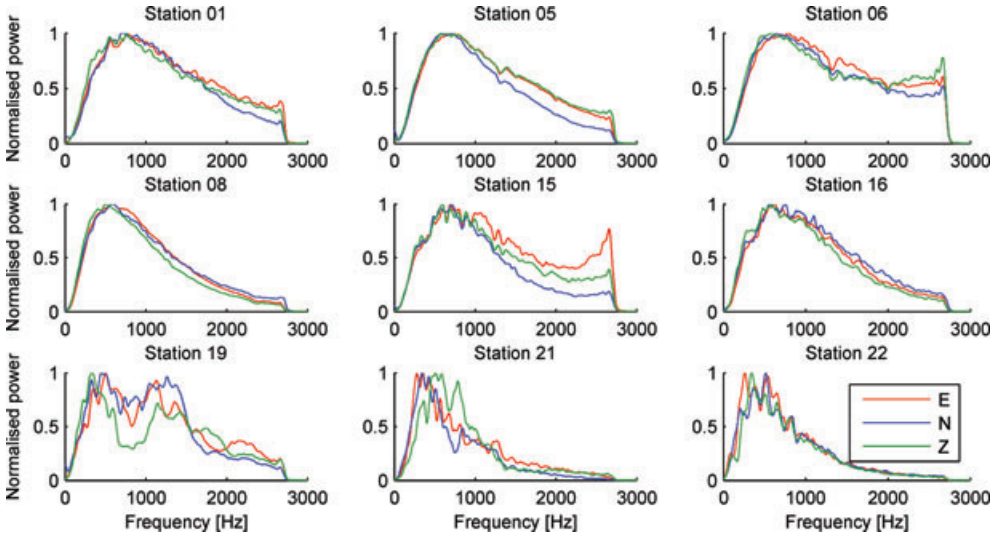

Figure 4. Cumulative frequency contents of the stations used in this study. For each component, we show the cumulative normalized frequency content of an *S*-wave window of all seismograms after electric noise reduction, again normalized to be comparable between stations.

where v_S is the mean *S*-wave velocity, dt is the splitting delay time and r is the source–receiver distance. Note that this represents a minimum estimate of bulk rock anisotropy. The experiment setup at Northparkes provides an ideal coverage of the seismogenic zone (Fig. 2). The large number of events allows resolution of the temporal evolution of the anisotropy throughout the recording period.

Fig. 7(a) shows the evolution of anisotropy during the study period. This represents the strength of shear wave anisotropy along a specific ray path and thus a minimum for a given anisotropic medium. Also shown is the seismicity in a 14-d sliding window. We observe an increase in anisotropy starting in mid-August, just as the seismicity rate increases. Following a peak at the beginning of November, the observed anisotropy decreases back to the level seen in mid-August.

This observation is consistent with an increase in fracturing during production, or at least with an increase in thickness of the fractured zone. Prior to cave initiation in 2004 mid-August, the events occur at a low seismicity rate throughout the whole monitored rock mass and thus map the background level of anisotropy (i.e. fracturing) of the rock. During production, most events occur close to the (upward) propagating cave back. The observed anisotropy reflects the newly developed, stress-induced fractures that form due to stress redistribution. After cave breakthrough in 2004 mid-December, the events again occur (at a low rate) outside the cave and thus again map the undisturbed rock.

4.1 Temporal or spatial variation?

A major issue encountered when interpreting observed variations in *S*-wave splitting, in both regional, mining and hydrocarbon reservoir anisotropy studies, is disentangling temporal changes in anisotropy from changes in spatial sampling of the subsurface. In simple terms, because the location of each source, and therefore the ray path, is different, observed splitting changes can be a function of either changing anisotropic strength/orientation, or of differing source locations. Different source regions will give different strengths of anisotropy because (1) the angle of propagation through the

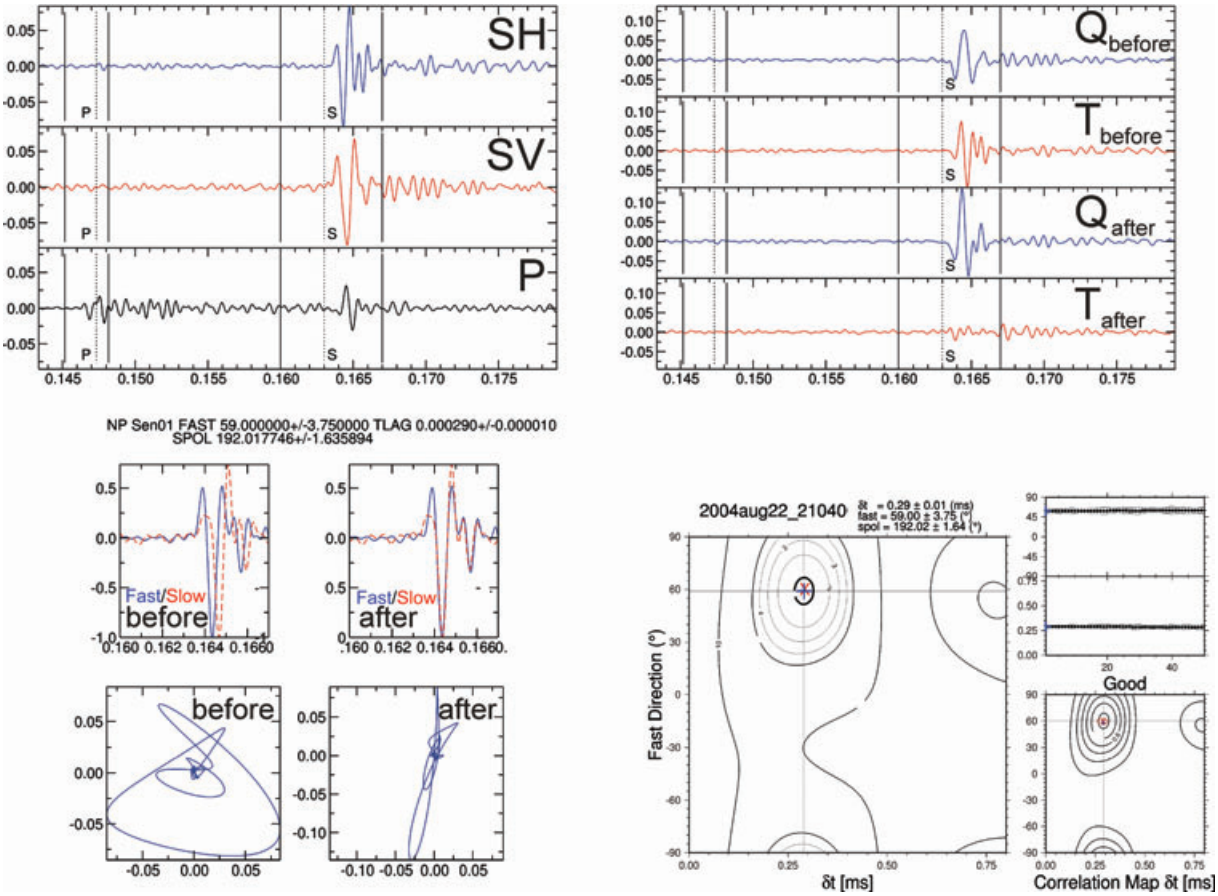

Figure 5. Example diagnostic plot of a shear wave splitting measurement from the Northparkes data set. Upper left panel shows the initial waveforms in *SH*, *SV*, *P* coordinates (blue, red and black, respectively). Upper right pannel shows *Q* (red) and *T* (blue) components before (upper two pannels) and after correction (lower two panles). Lower left panels shows in the top row fast (solid) and slow (dashed) *S* waves and in the bottom row particle motion in *SH*–*SV* coordinates, respectively, before and after correction. The lower right panel shows error surface plots for the eigenvalue and cross-correlation method with the minimum marked. Also shown is the variation of delay time and fast axis for the various test *S*-wave windows and the associated errorbars. For a detailed description see Wuestefeld *et al.* (2010).

subsurface is different or (2) the rock mass sampled by the wave is different.

We encounter this issue when interpreting the Northparkes data set—it may be difficult to distinguish temporal changes in anisotropy from spatial variations in pre-existing rock properties. It is possible that previous production in overlying layers de-stressed the roof, implying that the fractures we observe developing were already present at the beginning of this stage of mining. We only begin to observe them at later time steps because these more fractured zones become better illuminated, as the focus of seismicity moves higher. However, any fractures developed by mining in overlying areas are likely to be small compared to that induced by undercutting. Indeed, given that the ultimate result during undercutting is the total disintegration of the rock mass, it would be very surprising not to observe a temporal increase in the amount of fracturing.

By modelling the dependence of splitting on the angle of propagation, the inversion approach of Verdon *et al.* (2009) and Verdon & Kendall (2011) accounts for changes in the direction of propagation. However, it cannot account for the fact that later splitting measurements may sample a different proportion of the subsurface, which may have a different anisotropy, and therefore produce a varying anisotropic measurement without any need for temporal changes.

In Fig. 7(b), we plot the variation of observed anisotropy with depth. This variation is less pronounced and a correlation with seismicity is weaker than in the temporal analysis in Fig. 7(a). We thus interpret the depth variation being a consequence of temporal change, imposed by production. Due to the upward progression of the seismogenic front, it is not possible to completely disentangle temporal and spatial variation in shear wave splitting. We therefore separate the temporal variation (Fig. 7a) into several depth intervals (Fig. 8), with each panel of Fig. 8 representing events from within a 50-m depth interval. The deep intervals (>450 m depth) show no major variation of anisotropy in time, which can be interpreted as showing the (constant) background anisotropy of the rock mass. However, shallower depth intervals show strong temporal variations, which match the different production stages (compare intervals 350–400 and 225–275 m). This temporal change in anisotropy with depth indicates production-induced fracturing.

The good directional coverage of sensors allows illumination of anisotropy from a broad range of azimuths and inclinations at all times, that is, ray paths map similar portions of the mine throughout the experiment. If spatial variations were to account for our observed splitting variations, then the anisotropy must change as a function of depth. This style of spatial variation, although more common in hydrocarbon reservoirs with sedimentary layering, is difficult to

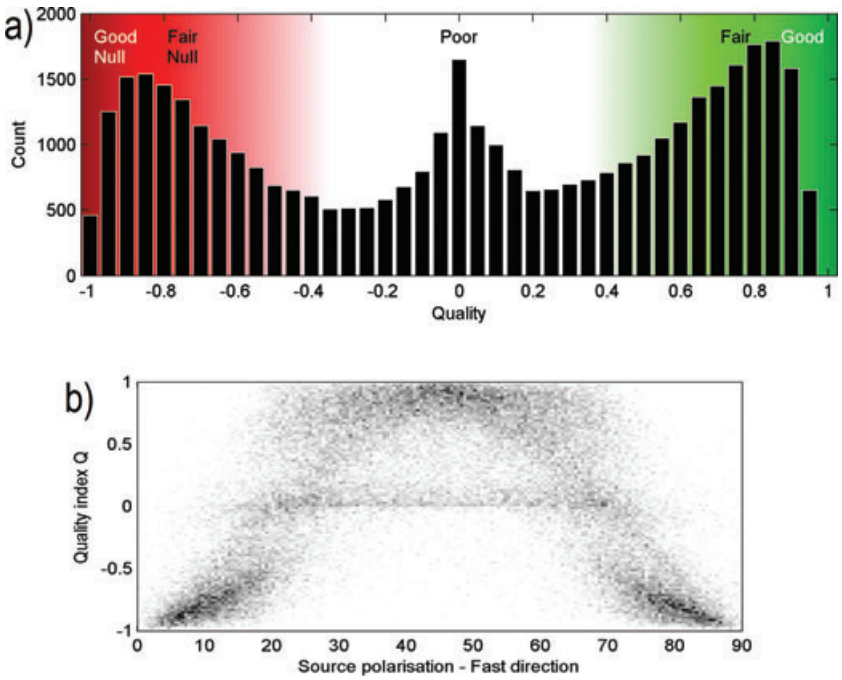

Figure 6. (a) Histogram of automatically determined shear wave splitting qualities for the Northparkes data set. (b) The quality density plot shows the distribution of splitting quality compared with the separation between initial polarization and seismic fast orientation. Note that a separation of approximately 15°–20° to provide good shear wave splitting results.

generate in a vertical dyke. Furthermore, the effect of the inversion technique described in Section 'Modelling of anisotrophy and fractures' is to 'average' the splitting from similar ray directions. We thus observe an average, homogeneous model for the mine. Since most events have ray paths within the ore body, the interpretation mainly reflects the ore body. We note that the anisotropy may be heterogeneous, which will complicate the interpretation of shear wave splitting (see Rumpker *et al.* 1999). A solution would be to address the issue with shear wave splitting tomography (e.g. Abt & Fischer 2008).

5 MODELLING OF ANISOTROPY AND FRACTURES

Illuminatingan anisotropic rock from various angles causes characteristic variation of fast shear wave polarization and delay times. This variation can be complex and ambiguous in orthorhombic or other, less symmetric anisotropy systems. Sileny & Plomerova (1996) and Verdon *et al.* (2009) used a grid search inversion to find the anisotropy model, which best fits the data. Verdon *et al.* (2009; 2011) use the additional compliance approach developed by Schoenberg & Sayers (1995) to model the elastic stiffness tensor of a rock mass with intrinsic anisotropy (induced by aligned minerals or thin sedimentary layers) that also contains multiple fracture sets. The additional compliance of a set of aligned fractures is a function of their orientation (dip and strike) and the fracture density (Hudson *et al.* 1996). The elastic stiffness tensor is then incorporated into the Christoffel equation to calculate shear wave in any given direction. The rms misfit between the splitting observations and those provided by the model is computed, and the values of model parameters that minimize misfit are selected as the most appropriate. By examining the misfit surface, the confidence intervals can be assigned, which show the uniqueness of the inversion—a tight, well-constrained minimum in the error surface implies a stable, unique inversion result.

As discussed earlier, block-caving operations are most effective in a rock with a near-vertical and a near-horizontal natural fracture set. We therefore modified the approach by Verdon *et al.* (2009) and invert for the three parameters horizontal crack density $\rho_{c,hori}$, vertical crack density $\rho_{c,vert}$, and strike of the vertical cracks φ_c. Each model is compared with the observed splitting parameter, minimizing the rms error to choose the best model. An F-test is used to compute the 90 per cent confidence interval of the inversion (Fig. 9). The variable seismicity and observed strength of anisotropy at Northparkes (Fig. 7a and Fig. 8) implies that inversions over multiple time windows are necessary to characterize the changing conditions through time. We thus selectively inverted the splitting parameters with $Q > 0.80$ within a 14-d sliding window in steps of 2 d. Only time windows containing more than 20 measurements are considered stable enough for the inversion. Fig. 9 shows detailed result plots of three examples of the inversion for 2004 August 31, November 3 and November 5 for a model of two fracture sets, oriented vertically and horizontally, respectively. The two fracture densities are well constrained in the first example, with higher horizontal than vertical fracture density. Fracture strike is at N70°E is slightly off the maximum horizontal stress direction (N96°E, Table 1), however with a confidence interval of 15°. In early November, the seismogenic zone reaches the crown pillar and breakthrough is completed on November 16. In the period leading to this breakthrough the inversion shows an abrupt change in horizontal fracture density and inverted fracture strike, which can be seen in Fig. 10(a). The inversion for November 3 shows this complexity by having a trade-off between horizontal and vertical fracture density (diagonally oriented error contour lines) and also a development of a secondary minimum. The strike is only poorly constrained. The error surface of strike of vertical fractures and horizontal fracture density develops a 'zigzag'

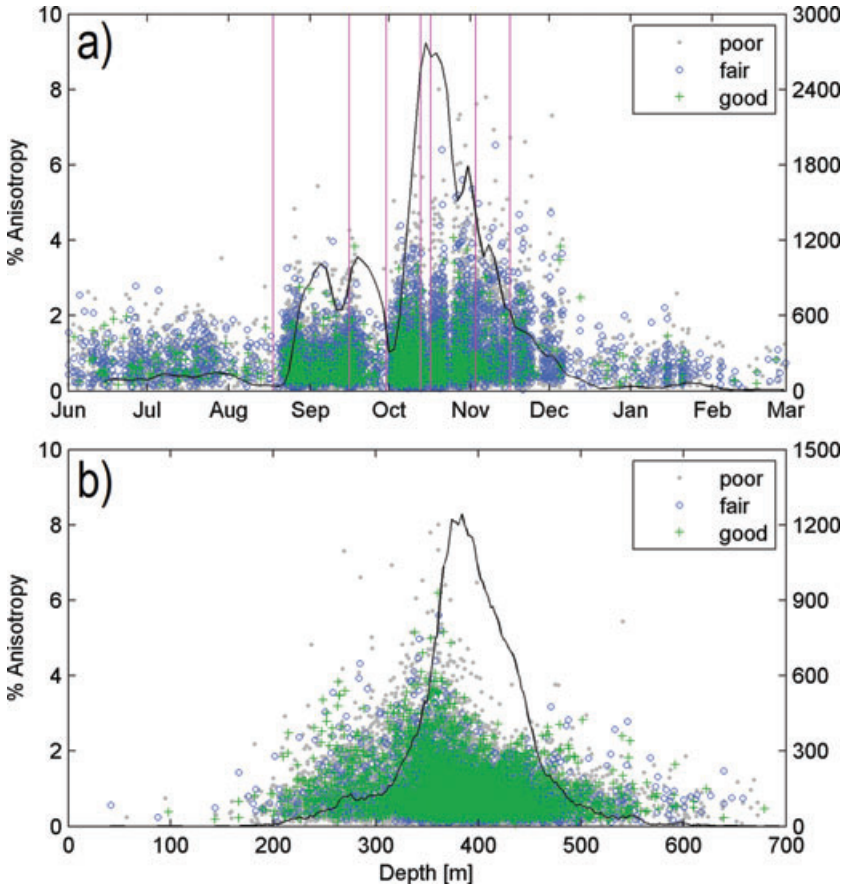

Figure 7. (a) Evolution of seismic anisotropy derived from good, fair and poor quality splitting measurements at Northparkes during excavation period. The solid line represents seismicity occurring within a 14-d sliding window. Note that the level of anisotropy is approximately 2 per cent before production starts in mid-August and then increases to 3.5 per cent. After a short halt in production at the end of September, production and seismicity increases significantly and the anisotropy reaches more than 6 per cent. After production halts in December, the background anisotropy of less than 2 per cent is observed as most events occur outside the seismogenic zone and thus map the surrounding rock. Vertical lines indicate major production events discussed in the text. (b) Variation of anisotropy with depth. Solid line indicates number of good measurements within a 5-m sliding depth window. Note that the spread in observed anisotropy is larger for shallower events.

shape, which is completed on the November 5 inversion. This behaviour indicates that the model of strictly vertical and horizontal fractures is insufficient to fully describe the nature of the fracturing. We thus infer that the breakthrough of the crown pillar has significantly different fracture mechanisms and thus stress conditions. Observations by Hudyma *et al.* (2007b; Fig. 3) of a period of large magnitude events supports this interpretation.

Fig. 10(b) shows the inversion for a second model simulating a single set of dipping fractures. Again, we observe an increase in fracture density, most significantly in the last stage of production in November, when approaching the crown pillar. The fracture dip is generally shallow at around 150°, supporting the previous findings of preferentially horizontal fractures (Fig. 10a). In the build-up to the breakthrough of the crown pillar (late October), the dip of this hypothesized single fracture gets gradually steeper and then returns back to 150°. The strike of shallow dipping planes is only poorly constrained for geometrical reasons. Sharp flips of the strike coincide with changes in production (machine breakdown in late September and breakthrough of the crown pillar late October). This may indicate that a single set of fracture cannot sufficiently explain the shear wave splitting pattern in these periods. Note that the fracture density for the dipping model increases significantly (Fig. 10b) at the same time as the vertical fracture density increases in the inversion for two fracture sets. This indicates a significant change in state of stress and eventually fractures mechanism.

6 INTERPRETATION

Our inversion of splitting parameters in the Northparkes Mine indicates an increase in fracturing during production, with more horizontally than vertically orientated fractures forming over that period. Production rate clearly influences fracture generation, as changes in fracture parameters correlate with seismicity rate (Fig. 10). Note that this is not an artefact of the inversion since we use a sliding window for the inversion. This sliding window may only account for some delay between changes in fracture parameters and seismicity rate.

For interpretation of the fracturing, we first recall basic fracture theory in a mining environment. Fractures are predicted to open perpendicular to minimum compressive stress, σ_3, and oriented along the orientation of the maximum compressive stress, σ_1. The intermediate stress orientation is denoted by σ_2 (Jaeger *et al.* 2007). Assuming these principal stress directions are oriented in

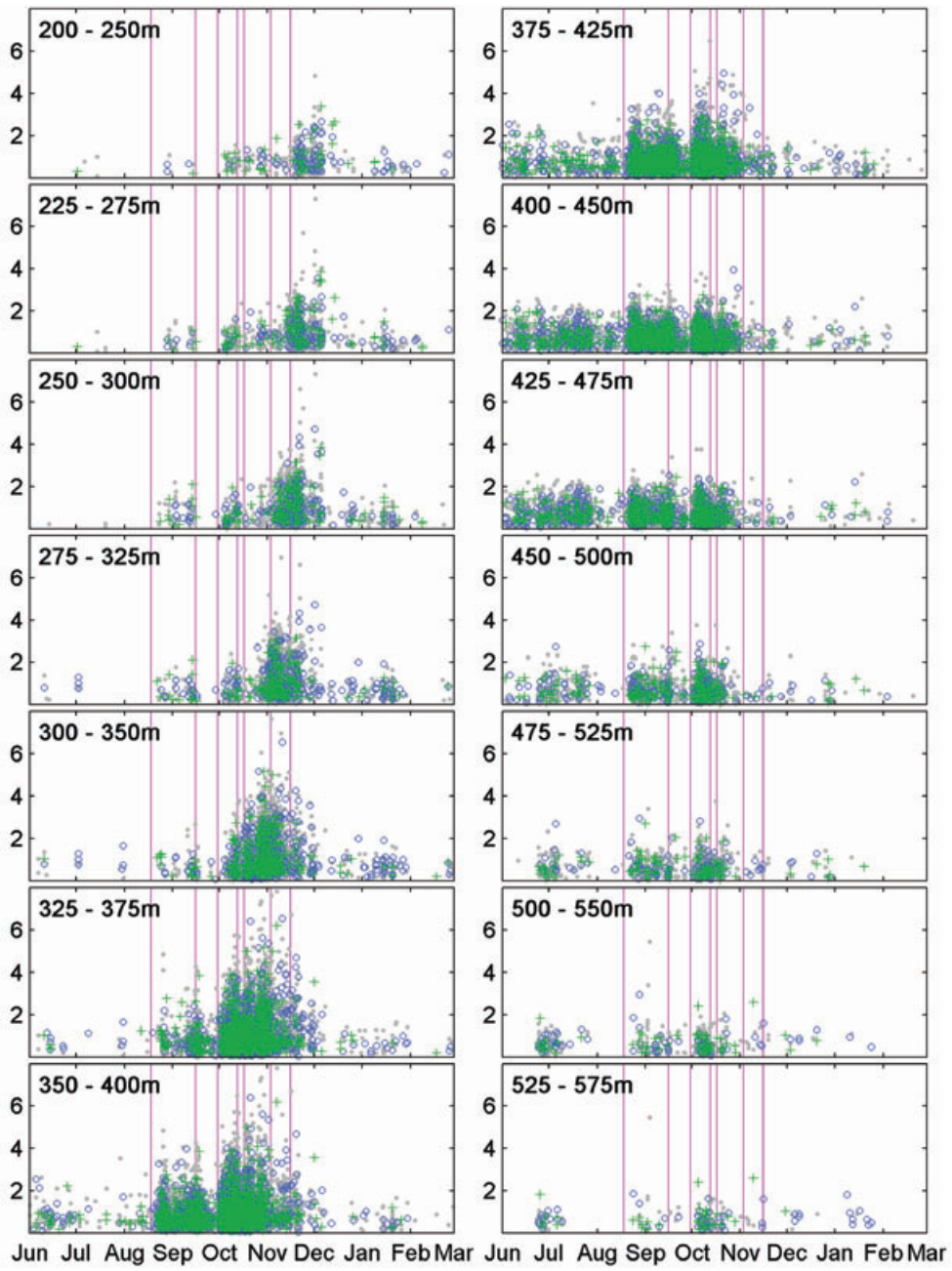

Figure 8. Temporal variation of anisotropy (in per cent) in various depth slices. See Figure 7 for details.

a geographical coordinate system (Anderson 1951), steep dipping normal faulting occurs if $\sigma_v > \sigma_H > \sigma_h$, where σ_v is the vertical stress, σ_H maximum horizontal stress and σ_h is the minimum horizontal stress orientation. When the stress field is very compressive, both horizontal stresses exceed the vertical stress and folding and (shallow dipping) thrust faulting could occur when $\sigma_H > \sigma_h > \sigma_v$. Note that dipping discontinuities are often associated with secondary structures. In crystalline rock, such stress condition results in near-vertical cracks and joints (Brady & Brown 1985; Pollard & Aydin 1988). Finally, strike-slip faulting represents an intermediate stress state, in which $\sigma_H > \sigma_v > \sigma_h$. We can thus conclude that the fracture regime can act as a guide for stress orientation and stress regime. For shallow mining (and tunnel) environments, the direction of least principal compressive stress is generally the vertical ($\sigma_3 = \sigma_V$). Measurements of *in situ* pre-mining stresses (Table 1) at the Northparkes Mine on the Lift 2 undercut level, 820 m below surface, support this assumption (Hudyma *et al.* 2007a, based on a technical report). Thus, near-horizontal stress-induced fracturing will occur above the scatter zone, which is parallel to the propagating cave back.

Near-vertical cracks also open due to a localized tensile stress regime ($\sigma_H > \sigma_v \geq 0 > \sigma_h$) in the roof of caves (Figs 1b and h). This stress regime is caused by the bending of the roof due to gravitational load of the overburden. Simultaneously, failure of the cave roof (referred to as 'cave collapse') results in conditions similar to borehole breakouts (e.g. Bell & Gough 1979; Zoback *et al.* 2003) and thus produces (tensile) near-horizontal fractures in the sidewalls of the cave. This is in line with observations of Oye *et al.*

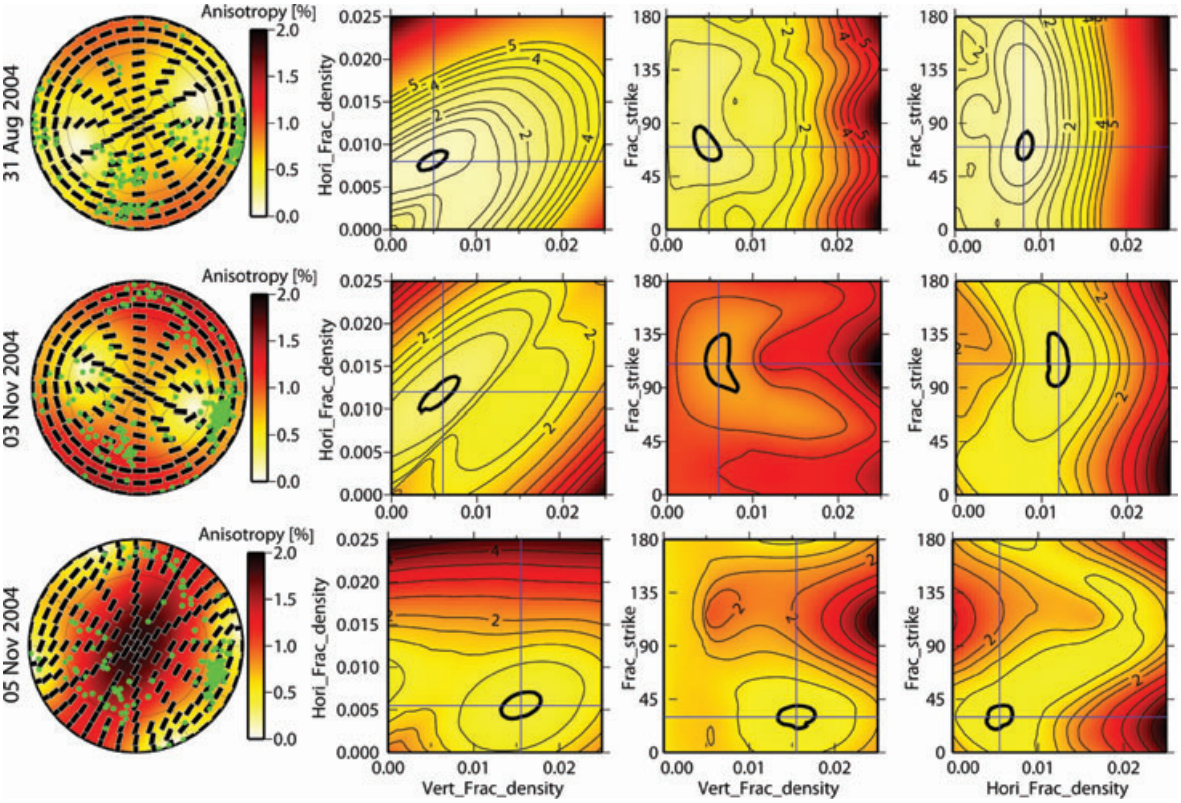

Figure 9. Example plots of the inversion for a test time window including events in a 14-d window before 2004 August 31, November 3 and November 5 at the Northparkes data set. These represent several stages of the production. On the left lower hemisphere, plot of phase arrivals show the directional coverage of the events used in inversion. The next three panels show error surface slices through the inversion data cube for the three parameters fracture strike, vertical and horizontal fracture density. Each slice is selected at the minimum of the, respectively, not shown parameter.

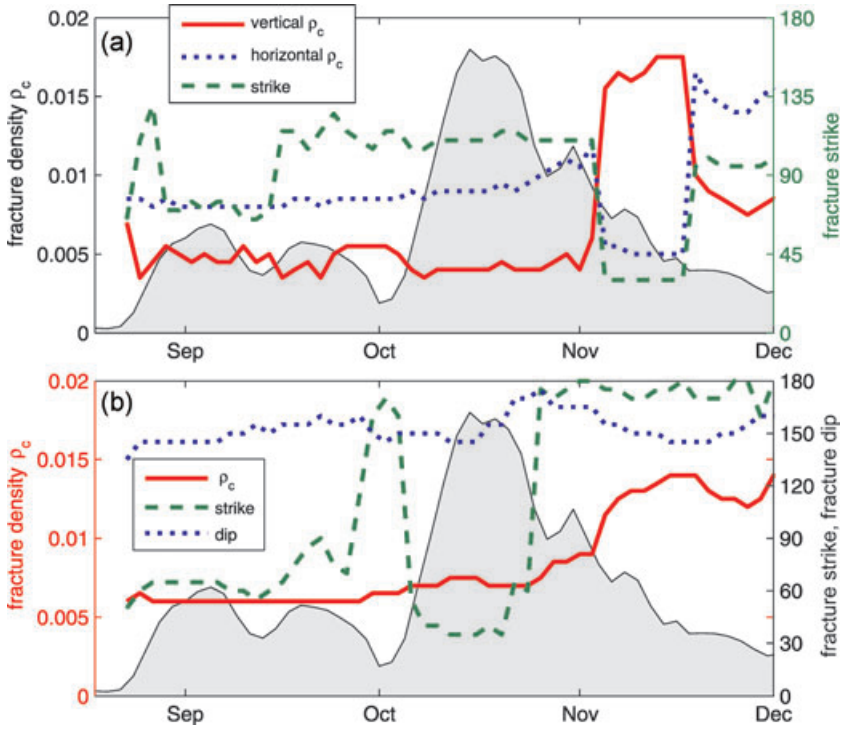

Figure 10. Evolution of fracture parameters during production period at Northparkes Mine. Shear wave splitting measurements within a 14-d sliding window are used for inversion. The seismicity in a 14-d sliding window is shown as gray shaded area for comparison. (a) Inversion of fracture parameters for two sets of fractures with horizontal and vertical orientations, respectively. b) Inversion for a single set of fractures but allowing the dip of the fracture set to vary.

Table 1. Pre-mining *in situ* stresses at Northparkes at a depth of 813 m below the surface (after Hudyma *et al.* 2007a).

Principal Stress component	Magnitude (Mpa)	Dip (°)	Azimuth (°)
σ_1	53.2	10	096
σ_2	33.1	01	186
σ_3	22.2	80	283

(2006) who find different source mechanism for spalling events which seem to relate to generally different stress drops for mining events. Similarly, Laboratory experiments (e.g. Haimson 2007) on borehole instability show microcracks opening subparallel to the borehole wall, that is, near-horizontal in the mining case. Haimson (2007) also describes flakes of rock 'peeling off' the breakouts at early stages similar to cave collapse. Again accepting that $\sigma_3 = \sigma_V$ in mining, this implies that subhorizontal fractures will open and the breakouts in caves will occur in the roof of the cave. The increase in horizontal fractures observed in the shear wave splitting measurements (Figs 10a and 11b) is thus consistent with a borehole breakout model with low vertical stress magnitude and tensile horizontal crack openings. These fracture orientations inverted from our microseismic study provide evidence that natural, horizontal joints and horizontal stress-induced fractures exist in the caving rock mass. Any pre-existing vertical and horizontal joints will be extended and eventually lead to failure of the rock mass above the cave back. Significant changes in fracture density (Figs 10a and b) coincide roughly with the breakthrough of the crown pillar. This breakthrough is associated with large magnitude events (Fig. 11c).

We estimate the average error of the fracture strike to approximately 20° (Fig. 9). Within this margin, the fractures are striking subparallel to $\sigma_1 = \sigma_H$, which is oriented E–W oriented prior to mining (Hudyma *et al.* 2007a; Table 1). This setup indicates a thrust regime as shown in Fig. 1(i), which is caused by small overburden. In block caving, the upward propagation of the cave roof effectively leads to a decrease in the overburden, and thus a decrease in σ_V. The sharp increase in vertical fracture density in late October may thus be explained by the breakthrough of the crown pillar, when in principle the rock strength is removed and thus the overburden is minimal.

Vertical fractures are also caused by the gravitational flexure of the roof, which locally will reduce σ_h, creating a local tensile stress regime $\sigma_H > \sigma_V > 0 > \sigma_h$. This is causing vertical cracks to open parallel to $\sigma_1 = \sigma_H$, which is E–W oriented. As the rock progressively fails (ultimately resulting in collapse) a localized tensional stress field is created in the vicinity of cracks and fractures, thus creating fractures which are dominantly vertical. This change in fracture mechanism is consistent with the change from a Gutenberg–Richter to a bimodal *b*-value distribution (Hudyma 2007b) as described earlier and indicates two types of frequency magnitude relationships. Further research on moment tensor solutions might reveal which faulting mechanisms are involved at which occurrence rate (Julia *et al.* 2009; Kuehn *et al.* 2009).

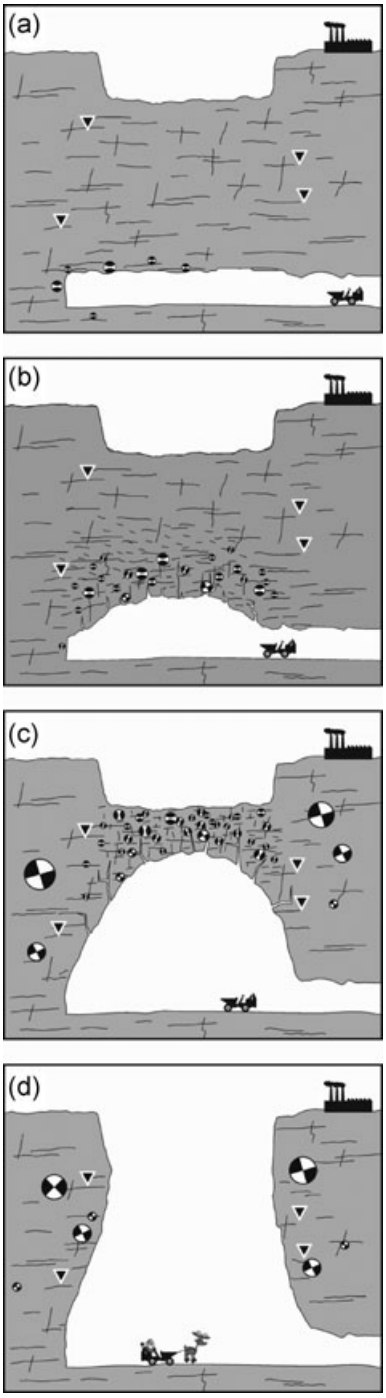

Figure 11. Cartoon of production and fracture evolution in the Northparkes Mine. Triangles indicate seismic stations. (a) few events occur around the new production tunnel and shear wave splitting records background fracturing of the rock. (b) In early excavation stages, tensile failure causes cave collapse and horizontal fractures are observed. (c) During breakthrough of the crown pillar, tensile failure in the roof is accompanied by shear failure in the cave wall. (d) After production large shear failures occur, and shear wave splitting maps again background fracturing.

7 CONCLUSION

We presented a shear wave splitting analysis of a large microseismic data set recorded in an Australian underground block cave mine. This data set has unprecedented ray coverage and the large number of events (more than 13 000 recorded at nine sensors) made it possible to analyse the temporal evolution of the anisotropy. A total of more than 40 000 splitting measurements were inverted for horizontal and vertical fracture parameters. We found that prior to production the 'natural' *S*-wave anisotropy of the rock is approximately 2 per cent. Caving causes most events to occur in the roof of the cave, where we observed an increase in fracturing of the

rock mass. This is manifested as an increase in the magnitude of anisotropy of up to 7 per cent. After cave breakthrough, the microseismicity is once again transferred to the surrounding rock mass and the observed anisotropy returns to ∼2 per cent. By analysing the anisotropy in depth-time intervals, as shown in Fig. 8, it might be possible to better monitor the rates of fracturing in mines. This could help guide mining strategies and help with hazard mitigation. Indeed one could envision real-time monitoring of fracture development in mines using our approach to automated shear wave splitting analyses.

An inversion of splitting parameters for fractures has shown how horizontally and vertically oriented fractures develop; in this case of block caving, the horizontally oriented fractures show a higher fracture density. A sharp increase in vertical fractures precedes crown pillar breakthrough, which we relate to a change in fracture mechanism from collapse-related tensile fracturing, to thrust faulting due to removal of the overburden. These findings could be better constrained with future work on focal mechanisms. We thus have shown how shear wave splitting can provide additional information about dominant fracture characteristics and orientation in a mine.

The observation of temporal changes in fracture properties is not only of importance in mining projects. Geoscience problems related to stress buildup also include borehole breakouts (e.g. Zoback *et al.* 2003) and volcanic activity, including caldera collapse (see Gudmundson 2006 for a review). The filling of a magma chamber is the inverse stress condition to generating a cavity and shear wave splitting shows promise as a useful monitoring tool (Gerst & Savage 2004). Shear wave splitting studies to analyse fractures are increasingly common on a crustal scale (see Crampin & Peacock 2008 for a review) and local scale (e.g. Teanby *et al.* 2004a; Rial *et al.* 2005; Al-Harrassi *et al.* 2011a,b). Here, we have shown how effective shear wave splitting analysis can be in characterizing fracture evolution in a dynamic environment.

ACKNOWLEDGMENTS

We thank the two reviewers Katrin Plenkers and Volker Oye as well as the Editor Wolfgang Friedrich, whose comments helped to greatly improve the manuscript.

REFERENCES

Abt, D.L. & Fischer, K.M., 2008. Resolving three-dimensional anisotropic structure with shear wave splitting tomography, *Geophys. J. Int.,* **173,** 859–886.

Al-Anboori, A., Kendall, J.M., Raymer, D. & Jones, R., 2005. Microseismic monitoring and spatial variations in anisotropy, an example from Oman, Extend. Abstr., in *Proceedings of the EAGE 67th Conference & Technical Exhibition*, Madrid, Spain, 13–16 June.

Al-Harrasi, O., Kendall, J-M. & Chapman, M., 2011a. Fracture characterisation using frequency-dependent shear-wave anisotrophy analysis of microseismic data, *Geophys. J. Int.,* **185,** 1059–1070.

Al-Harrasi, O., Al-Anboori, A., Wuestefeld, A. & Kendall, J.M., 2011b. Seismic anisotropy in a hydrocarbon field estimated from microseismic data, *Geophys. Prospect.,* **73**(2), 227–243.

Al-Harrasi, O., Kendall, J-M. & Chapman, M., 2011b. Fracture characterisation using frequency-dependent shear-wave anisotropy analysis of microseismic data, *Geophys. J. Int.,* doi:10.1111/j.1365-246X.2011.04997.x.

Allegre, C.J., Le Mouel, J.L. & Provos, A., 1982. Scaling rules in rock fracture and possible implications for earthquake prediction, *Nature,* **297,** 47–49.

Anderson, E.M, 1951. *The Dynamics of Faulting and Dyke Formation with Applications to Britain,* Oliver & Boyd, Edinburgh.

Backus, G.E., 1965. Long-wave elastic anisotropy produced by horizontal layering, *J. geophys. Res.,* **67,** 4427–4440.

Baisch, S., Vörös, R. Weidler, R. & Wyborn, D., 2009. Investigation of fault mechanisms during geothermal reservoir stimulations experiments in the Cooper Basin, Australia, *Bull. seism. Soc. Am.,* **99**(1), 148—158.

Barruol, G. & Hoffmann, R., 1999. Upper mantle anisotropy beneath the Geoscope stations, *J. geophys. Res.,* **104**(B5), 10 757–10 773.

Bell, J. & Gough, D., 1979. Northeast-southwest compressive stress in Alberta evidence from oil wells, *Earth planet. Sci. Lett.,* **45**(2), 475–482.

Blackman, D.K., Wenk, H-R. & Kendall, J-M., 2002. Seismic anisotropy of the upper mantle: 1. Factors that affect mineral texture and effective elastic properties, *Geochem. Geophys. Geosyst.,* **3**(9), 8601, doi:10.1029/2001GC000248.

Boettcher, M.S., McGarr, A. & M. Johnston (2009), Extension of Gutenberg-Richter distribution to M_W -1.3, no lower limit in sight, *Geophys. Res. Lett.,* **36,** L10307, doi:10.1029/2009GL038080.

Brace, W.F., Paulding, B. & Scholz, C.H., 1966. Dilatancy in the fracture of crystalline rocks, *J. geophy. Res.,* **71,** 3939–3953.

Brady, B.H.G. & Brown, E.T., 1985. *Rock Mechanics for Underground Mining,* George Allen & Unwin, London.

Butler, K.E. & Russelly, R.D., 2003. Cancellation of multiple harmonic noise series in geophysical records, *Geophysics,* **68,** 1083–1090.

Crampin, S., 1984. Effective anisotropic elastic constants for wave propagation through cracked solids, *Geophys. J. R. astr. Soc.,* **76**(1), 135–145.

Crampin, S. & Peacock, S., 2008. A review of the current understanding of seismic shear-wave splitting in the Earth's crust and common fallacies in interpretation, *Wave Motion,* **45,** 675–722.

Cypser, D.A. & Davis, S.D., 1998. Induced seismicity and the potential for liability under U.S. law, *Tectonophysics,* **289**(1–3), 239–255.

Dorbath, L., Cuenot, N., Genter, A. & Frogneux, M., 2009. Seismic response of the fractured and faulted granite of Soultz-sous-Forets (France) to 5 km deep massive water injections, *Geophys. J. Int.,* **177**(2), 653–675.

Gay, N.C. & Ortlepp, W.D., 1979. Anatomy of a mining-induced fault zone, *Bull. geol. Soc. Am.,* **90**(1), 47–58.

Gerst, A. & Savage, M.K., 2005. Seismic anisotrophy beneath Ruapehu volcano: a possible eruption forecasting tool, *Science,* **306,** 1543–1547.

Gibowicz, S.J. & Kijko, A., 1994. *An Introduction to Mining Seismology,* Academic Press, New York.

Gudmundson, A., 2006. How local stresses control magma-chamber ruptures, dyke injections, and eruptions in composite volcanoes, *Earth-Sci. Rev,* **79,** 1–31.

Gutenberg, B. & Richter, C.F., 1944. Frequency of earthquakes in California, *Bull. seism. Soc. Am.,* **34,** 185–188.

Haimson, B., 2007. Micromechanisms of borehole instability leading to breakouts in rocks, *Int. J. Rock Mech. Min. Sci.,* **44**(2), 157–173.

Hall, S.A., Kendall, J-M., Maddock, J. & Fisher, Q., 2008. Crack density tensor inversion for analysis of changes in rock frame architecture, *Geophys. J. Int.,* **173,** 577–592, doi:10.1111/j.1365-246X.2008.03748.x.

Hasegawa, H.S., Wetmiller, R.J. & Gendzwill, D.J., 1989. Induced seismicity in mines in Canada—an overview, *Pageoph,* **129**(3), 423–453.

Holmes, G.M. Crampin, S. & Young, R.P., 1993. Preliminary analysis of shear-wave splitting in granite at the Underground Research Laboratory, Manitoba, *Can. J. Explor. Geophys.,* **29,** 140–152.

Holmes, G.M. Crampin, S. & Young, R.P., 2000. Seismic anisotropy in granite at the Underground Research Laboratory, Manitoba, *Geophys. Prospect.,* **48**(3), 415–435.

Hudson, J.A., Liu, E. & Crampin, S., 1996. The mechanical properties of materials with interconnected cracks and pores, *Geophys. J. Int.,* **124,** 105–112.

Hudyma, M., Potvin, Y. & Allison, D., 2007a. Seismic monitoring of the Northparkes Lift 2 block cave: part 1. Undercutting, in *Proceedings of the 1st International Symposium on Block and Sub-Level Caving,* ed. Potvin, Y., The S. African Institute of Mining and Metallurgy, pp. 303–334.

Hudyma, M., Potvin, Y. & Allison, D., 2007b. Seismic monitoring of the Northparkes Lift 2 block cave: part 2. Production caving, in *Proceedings of the 1st International Symposium on Block and Sub-Level Caving,*

ed. Potvin, Y., The S. African Institute of Mining and Metallurgy, pp. 335–354.

Jaeger, J.C., Cook, N.G.W. & Zimmerman, R.W., 2007. *Fundamentals of Rock Mechanics,* 4th edn, Blackwell Publ. Ltd., Oxford.

Julia, J., Nyblade, A.A., Durrheim, R., Linzer, L., Gok, R., Dirks, P & Walter, W., 2009. Source mechanisms of mine-related seismicity, Savuka Mine, South Africa, *Bull. seism. Soc. Am.,* **99**(5), 2801–2814.

Kendall, J.-M., Pilidou, S., Keir, D., Bastow, I.D., Stuart, G.W. & Ayele, A., 2006. Mantle upwellings, melt migration and the rifting of Africa: insights from seismic anisotropy, in *The Afar Volcanic Province within the East African Rift System,* pp. 55–72, eds Yirgu, G., Ebinger, C.J. & Maguire, P.K.H., Special Publication, Geol. Soc., London.

Kendorski, F.S., 1978. The capability of ore deposits, *Min. Eng.,* **30,** 628–631.

Kuehn, D., Gharti, H.N., Oye, V. & Roth, M., 2009. Automatic determination of full moment tensor solutions from P-wave first motion amplitudes, in *Proceedings of the EAGE Passive Seismic Workshop—Exploration and Monitoring Applications,* Limassol, Cyprus.

Kwiatek, G., Plenkers, K., Nakatani, M., Yabe, Y. & Dresen, G., 2010. Frequency-magnitude characteristics down to magnitude –4.4 for induced seismicity recorded at Mponeng Gold Mine, South Africa, *Bull. seism. Soc. Am.,* **100**(3), 1165–1173.

Laubscher, D., 1994. Cave mining: the state of the art, *J. South Afr. Inst. Min. Metall.,* **94,** 279–293.

Lockner, D., 1994. The role of acoustic emission in the study of rock fracture, *Int. J. Rock Mech. Min. Sci. Geomech. Abstr.,* **30**(7), 883–899.

McGarr, A., 1971a, Stable deformation of rock near deep-level tabular excavations, *J. geophys. Res.,* **76**(29), 7088–7106.

McGarr, A., 1971b, Violent deformation of rock near deep-level, tabular excavations-seismic events, *Bull. seism. Soc. Am.,* **61**(5), 1453–1466.

Mikula, P., 2005. The practice of seismic management in mines: how to love your seismic monitoring system, in *Proceedings of the Sixth International Symposium on Rockburst and Seismcity in Mines (RASIM6),* eds Potvin, Y. & Hudyma, M., Australian Centre for Geomechanics, pp. 21–31.

Mintrop, L., 1909. Die Erdbebenstation der Westfälischen Berggewerkschaftskasse in Bochum, *Glueckauf,* **45,** 357–365.

Nur, A. & Simmons, G., 1969. Stress-induced velocity anisotropy in rock: an experimental study, *J. geophys. Res.,* **74,** 6667–6674.

Oye, V., Roth, M. & Bungum, H., 2006. Source parameters determined from microearthquakes in an underground ore mine, in *Earthquakes: Radiated Energy and the Physics of Faulting,* Vol. **170,** pp. 75—80, eds Abercombie, R., McGarr, A., Kanamori, H. & Di Torro, G., AGU Geophysical Monograph Series.

Parsons, T. & Geist, E.L., 2009. Is there a basis for preferring characteristic earthquakes over a Gutenberg-Richter distribution in probabilistic earthquake forecasting? *Bull. seism. Soc. Am.,* **99**(3), 2012–2019.

Phillips, W.S., Fairbanks, T.D., Rutledge, J.T. & Anderson, D.W., 1998. Induced microearthquake patterns and oil-producing fracture systems in the Austin chalk, *Tectonophysics,* **289**(1–3), 153–169.

Phillips, W., Rutledge, J., House, L. & Fehler, M., 2002. Induced microearthquake patterns in hydrocarbon and geothermal reservoirs: six case studies, *Pageoph,* **159**(1), 345–369.

Plenkers, K., Kwiatek, G., Nakatani, M. & Dresen, G., 2010. Observation of seismic events with frequencies $f > 25$ kHz at Mponeng Deep Gold Mine, South Africa, *Seismol. Res. Lett.,* **81**(3), 467–479.

Pollard, D.D. & Aydin, A., 1988. Progress in understanding jointing over the past century, *Bull. geol. Soc. Am.,* **100,** 1181–1204.

Potvin, Y., 2009. Strategies and tactics to control seismic risks in mines, *J. South Afr. Inst. Min. Metall.,* **109**(3), 177–186.

Reches, Z. & Lockner, D.A., 1994. Nucleation and growth of faults in brittle rocks, *J. geophys. Res.,* **99**(B9), 18 159–18 173

Rial, J.A., Elkibbi, M. & Yang, M., 2005. Shear-wave splitting as a tool for the characterization of geothermal fractured reservoirs: lessons learned, *Geothermics,* **34**(3), 365–385.

Rümpker, G., Tommasi, A. & Kendall, J-M. 1999. Numerical simulations of depth-dependent anisotropy and frequency-dependent wave propagation effects, *J. geophys. Res.,* **104,** 23 141–23 153.

Savage, M.K., 1999. Seismic anisotropy and mantle deformation: what have we learned from shear wave splitting, *Rev. Geophys.,* **37,** 69–106.

Schoenberg, M.A., 2009. Vertically fractured transversely isotropic media: dimensionality and deconstruction, *Geophys. Prospect.,* **57,** 169–185.

Schoenberg, M. & Sayers, C.M., 1995. Seismic anisotropy of fractured rock, *Geophysics,* **60,** 204–211.

Schorlemmer, D., Weimer, S. & Wyss, M., 2005. Variation in earthquake-sized distribution across different stress regimes, *Nature,* **437,** 539–542.

Sileny, J. & Plomerova, J., 1996. Inversion of shear-wave splitting parameters to retrieve three-dimensional orientation of anisotropy in continental lithosphere, *Phys. Earth planet. Inter.,* **95,** 277–292.

Silver, P.G., 1996. Seismic anisotropy beneath the continents: probing the depths of geology, *Annu. Rev. Earth planet. Sci.,* **24,** 385–432.

Simpson, D.W., 1986. Triggered earthquakes, *Annu. Rev. Earth planet. Sci.,* **14,** 21–42.

Spottiswoode, S.M. & Milev, A.M., 1998. The use of waveform similarity to define planes of mining-induced seismic events, *Tectonophysics,* **289**(1), 51–60.

Teanby, N.A., Kendall, J.-M., Jones, R.H. & Barkved, O., 2004a. Stress-induced temporal variations in seismic anisotropy observed in microseismic data, *Geophys. J. Int.,* **156,** 459–466.

Teanby, N.A., Kendall, J.-M. & van der Baan, M., 2004b. Automation of shear-wave splitting measurements using cluster analysis, *Bull. seism. Soc. Am.,* **94**(2), 453–463.

Trifu, C.-I., Angus, D. & Shumila, V., 2000. A fast evaluation of the seismic moment tensor for induced seismicity, *Bull. seism. Soc. Am.,* **90**(6), 1521–1527.

Trueman, R., Pierce, M. & Wattimena, R., 2002. Quantifying stresses and support requirements in the undercut and production level drifts of block and panel caving mines, *Int. J. Rock Mech. Min. Sci.,* **39**(5), 617–632.

Urbancic, T.I. & Rutledge, J., 2000. Using microseismicity to map cotton valley hydraulic fractures, *SEG Expanded Abstr.,* **19,** 1444–1448.

Valcke, S.L.A., Casey, M., Lloyd, G.E., Kendall, J.-M. & Fisher, Q.J., 2006. Lattice preferred orientation and seismic anisotropy in sedimentary rocks, *Geophys. J. Int.,* **166,** 652–666.

Vega, S., Mavko, G., Prasad, M. & Nur, A., 2006. Detection of stress-induced velocity anisotropy in unconsolidated sands, *Leading Edge,* **25**(3), 252–256.

Verdon, J.P. & Kendall, J-M., 2011. Detection of multiple fracture sets using observations of shear-wave splitting in microseismic data, *Geophys. Prospect.,* doi:10.1111/j.1365-2478.2010.00943.x.

Verdon, J.P., Angus, D.A., Kendall, J.M. & Hall, S.A., 2008. The effect of microstructure and nonlinear stress on anisotropic seismic velocities, *Geophysics,* **73**(4), D41–D51.

Verdon, J.P., Kendall, J.-M. & Wuestefeld, A., 2009. Imaging fractures and sedimentary fabrics using shear wave splitting measurements made on passive seismic data, *Geophys. J. Int.,* **179**(2), 1245–1254.

Verdon, J.P., White, D.J., Kendall, J.M., Angus, D. Fisher, Q. & Urbancic, T., 2010. Passive seismic monitoring of carbon dioxide storage at Weyburn, *Leading Edge.* **29**(2), 936–942.

Wesnousky, S.G., 1994. The Gutenberg-Richter or characteristic earthquake distribution, which is it?, *Bull. seism. Soc. Am.,* **84**(6), 1940–1959.

Wuestefeld, A. & Bokelmann, G., 2007. Null detection in shear-wave splitting measurements, *Bull. seis. Soc. Am.,* **97**(4), 1204–1211.

Wuestefeld, A., Bokelmann, G., Barruol, G. & Montagner, J.-P., 2009. Identifying global seismic anisotropy patterns by correlating shear-wave splitting and surface-wave data, *Phys. Earth planet. Inter.,* **176**(3–4), 198–212.

Wuestefeld, A., Al-Harrasi, O., Verdon, J.P., Wookey, J. & Kendall, J.M., 2010. Strategies for a fully automated passive microseismic anisotropy analysis, *Geophys. Prospect.,* **58**(5), 755–773.

Zoback, M.D. *et al*., 2003. Determination of stress orientation and magnitude in deep wells, *Int. J. Rock Mech. Min. Sci.,* **40**(7–8), 1049–1076.